

# RSC Advances



This is an *Accepted Manuscript*, which has been through the Royal Society of Chemistry peer review process and has been accepted for publication.

*Accepted Manuscripts* are published online shortly after acceptance, before technical editing, formatting and proof reading. Using this free service, authors can make their results available to the community, in citable form, before we publish the edited article. This *Accepted Manuscript* will be replaced by the edited, formatted and paginated article as soon as this is available.

You can find more information about *Accepted Manuscripts* in the [Information for Authors](#).

Please note that technical editing may introduce minor changes to the text and/or graphics, which may alter content. The journal's standard [Terms & Conditions](#) and the [Ethical guidelines](#) still apply. In no event shall the Royal Society of Chemistry be held responsible for any errors or omissions in this *Accepted Manuscript* or any consequences arising from the use of any information it contains.

## Nanocomposite $\text{CuCO}_3\text{-CuO}$ as a novel and environmentally friendly catalyst for triazole synthesis.

Halima Hadj Mokhtar <sup>a,b</sup>, Bouhadjar Boukoussa <sup>c,d\*</sup>, Rachida Hamacha <sup>c</sup>, Abdelkader Bengueddach <sup>c</sup>, Douniazad El Abed <sup>a</sup>.

<sup>a</sup>Laboratoire de Réactivité et Chimie Fine L.C.F, Université d'Oran 1 Ahmed Ben Bella, BP 1524 El M'naouer, 31100 Oran, Algeria.

<sup>b</sup>Centre de Recherche Scientifique et Technique en Analyses Physico-Chimiques (C.R.A.P.C), BP 384, Bou-Ismaïl RP 42004 Tipaza, Algeria.

<sup>c</sup>Laboratoire de Chimie des Matériaux L.C.M, Université d'Oran1 Ahmed Ben Bella, BP 1524 El-Mnaouer, 31000 Oran, Algeria.

<sup>d</sup>Centre Universitaire Ain Témouchent, Institut des Sciences et de la Technologies, BP 284, 46000 Ain Témouchent, Algeria

\*Corresponding author. Tel: +213771663458.

E-mail addresses: [bbouhdjer@yahoo.fr](mailto:bbouhdjer@yahoo.fr)

### Abstract:

This paper focuses on the use of natural sources for the preparation of efficient and low cost catalysts. The  $\text{CaCO}_3$  material is obtained from the bone of cuttlefish that was modified by cation exchange of  $\text{Ca}^{++}$  by  $\text{Cu}^{++}$  in  $\text{CaCO}_3$  using a solution of copper ( $\text{Cu}(\text{NO}_3)_2$ ) at different concentrations. The modification of solids was investigated by X-ray diffraction (XRD), Fourier transform infrared spectroscopy (FTIR), scanning electronic microscopy (SEM), the energy dispersive spectrometry (EDS) and ultraviolet–visible (UV–vis) spectroscopy. The results show that the copper exchanged materials contain nanoparticle composite  $\text{CuCO}_3\text{-CuO}$ . The obtained solids were used as catalysts for cycloaddition reaction of different azides with activated alkenes at room temperature under liquid-phase conditions. The different parameters which affect the reaction were investigated such as reaction time, temperature reaction, effect of copper content, catalyst mass, effect of solvent and nature of azide. High yields were obtained with the catalyst containing more amount of copper. The best catalysts were calcined at different temperatures 200, 300, 400,

500°C in order to determine the active phase  $\text{CuCO}_3$  or  $\text{CuO}$  in the catalytic reaction. The XRD analysis of calcined composites show that the increase in calcination temperature leads to the formation of the  $\text{CuO}$  phase. On the other hand, the use of these calcined materials as catalysts shows that the active phase is copper carbonate. Finally, a new method for preparing triazoles in short reaction times was developed by the use of cheap environmentally friendly catalyst.

**Keywords:**  $\text{CaCO}_3$ , Copper carbonate, Cycloaddition reaction, Triazoles synthesis, Catalyst re-use.

## 1. Introduction

During the last decades, the manufacturing of inorganic materials with specific size, morphology and crystallinity are considered as the factor responsible for their properties.<sup>1-3</sup> To date, the scientists focused on the synthesis of ordered structures with different morphologies and structures assembled by nanostructures 1D and 2D which have a great interest to chemists and materials scientists for their new properties and fundamental importance in the practical applications areas.<sup>4</sup> Recently, considerable effort has been devoted to investigate effective methods of synthesis of porous materials including free procedures in one step and simple catalyst are highly desirable.<sup>5</sup>

$\text{CaCO}_3$  is the most abundant crystalline biomineral which has drawn the attention of researchers because of its different morphologies such as needle-shaped,<sup>6</sup> nanospheres, rhombohedral-shaped,<sup>7</sup> lens-shaped and hexagonal-shaped,<sup>8</sup> microspheres with urchin-shaped structure.<sup>9</sup> This material proved to be a suitable catalyst or catalyst support for different reaction such as degradation of Acid Red B,<sup>10</sup> propylene epoxidation,<sup>11</sup> oxidation of 1,2-dichlorobenzene,<sup>5</sup> biodiesel production,<sup>12-14</sup>

homocoupling of aromatic halides,<sup>15</sup> decomposition of acetylene,<sup>16</sup> photo-catalysis of COD,<sup>17</sup> Fischer–Tropsch synthesis.<sup>18</sup>

The carbonate-based materials involve a large variety of cations such as Ca, Mg, Fe, Cu or Mn leading to different composition for examples CaCO<sub>3</sub>, MgCO<sub>3</sub>, CuCO<sub>3</sub>, FeCO<sub>3</sub>, MnCO<sub>3</sub>. The proprieties of these materials allow them to be used in a large applications in food and pharmaceutical industries, and also as filler in paper, plastic materials, in catalysis, adsorption, medicine, electronics, ceramics, optic, energy, magnetic, pigments and cosmetics.<sup>18-25</sup> The use of matrices containing copper in the catalysis field has received much attention in the last decades, due to the important basicity and potential redox of copper,<sup>26-28</sup> the synthesis of a hybrid material CuCO<sub>3</sub>-CuO is much easy by using copper precipitation method in the medium containing the CaCO<sub>3</sub> or Na<sub>2</sub>CO<sub>3</sub>,<sup>29-31</sup> and the use of heating promotes the transformation of CuCO<sub>3</sub> to CuO, this gives a perspective on the use of these solids in different fields mainly in heterogeneous catalysis.

In the last years many publications were focused on the synthesis of triazoles, these organic products have been interesting in the development of novel compounds with anticonvulsant, antidepressant, antioxidant, anti-inflammatory, analgesic, antinociceptive, antibacterial, antimycobacterial, antifungal, antiviral, anticancer, anti-parasitic, anti-urease and other activities.<sup>32-35</sup> There are many methods for preparing triazole derivatives that have been developed,<sup>36,37</sup> the use of heterogeneous catalytic system benefits from considerable synthetic advantages, easy availability of starting materials, short durations of reaction, simplicity of the reaction procedure, efficient catalyst for regeneration and separation.<sup>38</sup> Heterogeneous catalysts based on copper are considerably preferred for these type of reaction due to the presence of Cu<sup>++</sup>. For the purpose to obtain the best catalytic performance for cycloaddition reactions,

different catalysts based on copper are described in the literature such as: Cu/mesoporous materials,<sup>39,40</sup> copper nanoparticles (Cu NPs),<sup>41</sup> zeolite supported copper nanoparticles,<sup>42</sup> Cu/chitosan,<sup>43</sup> Cu/polymer catalysts<sup>44</sup> and others....

This work focuses on the facile and low cost synthetic method that leads to the direct transformation of  $\text{CaCO}_3$  to  $\text{CuCO}_3\text{-CuO}$  nanostructured materials by precipitation of  $\text{CaCO}_3$  in a solution containing  $\text{Cu}(\text{NO}_3)_2$ . Furthermore, the cycloaddition reaction of different azides catalyzed by  $\text{CuCO}_3\text{-CuO}$  was also discussed based on experimental evidence. This contribution will also provide new insights into better understanding the reaction kinetics for cycloaddition of azide-activated alkenes.

## 2. Experimental

### 2.1. Preparation procedure for catalysts

The material  $\text{CaCO}_3$  was obtained from cuttlefish bone, it was recovered in the seashore areas in Ain el turck Oran Algeria, see Fig.1. After grinding the solid and washing with ethanol to remove all organic traces, the recovered powder was treated by solutions containing different concentrations of  $\text{Cu}(\text{NO}_3)_2$ . After a few minutes stirring the product is formed as attested by the appearance of a blue precipitate. The obtained materials were filtered, washed and dried at 353K. The concentrations of copper nitrate solutions employed for the preparation of catalysts are : 1M, 0.8 M, 0.6 M, 0.4 M and 0.2 M, and the formed products are respectively named : MB1, MB0.8, MB0.6, MB0.4, MB0.2 and MB0 ( $\text{CaCO}_3$  before treatment with copper solution).

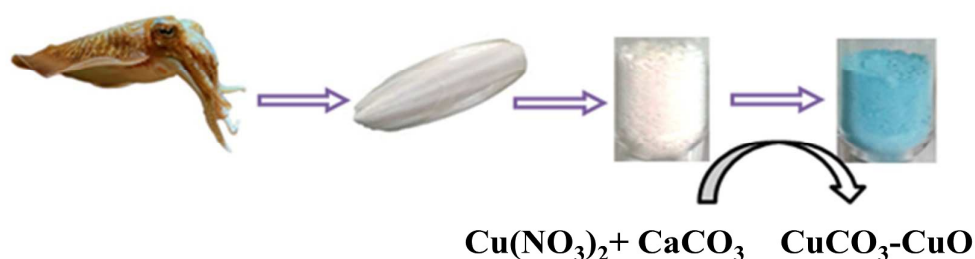
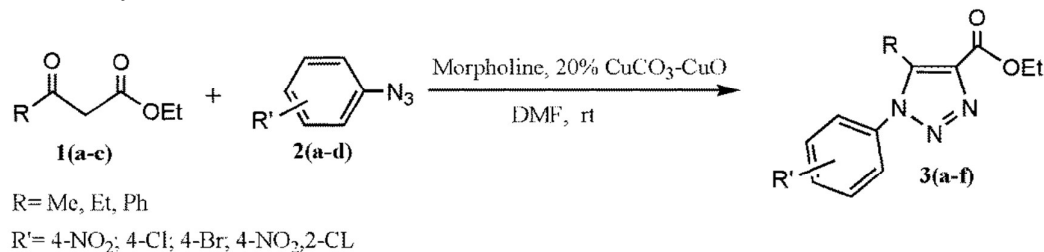


**Fig.1.** Preparation of nanocomposite  $\text{CuCO}_3\text{-CuO}$  using cuttlefish bone.

## 2.2. Catalytic test:



**Scheme 1:** Cycloaddition reaction of arylazides and activated alkenes using nanocomposite CuCO<sub>3</sub>-CuO catalyst.

The catalytic reaction involves the preparation of solution containing arylazides (1mmol) in DMF (1mL) (see scheme 1), then was firstly added activated alkenes (1mmol) and morpholine (1mmol) then the catalyst CuCO<sub>3</sub>-CuO (20mol%). The mixture was stirred 1.5-4 h at room temperature. After completion of the reaction, the precipitate formed upon addition of H<sub>2</sub>O (10 mL) was filtrated, washed with H<sub>2</sub>O and dried. To remove the catalyst, the precipitate was extracted with ethylacetate. After removal of the solvent, the crude product was recrystallized (by EtOH).

## 2.3. Characterization

The XRD powder diffraction patterns of the CaCO<sub>3</sub> and CuCO<sub>3</sub>-CuO nanocomposite materials were obtained with a Bruker D8 Advance X-Ray diffractometer (40 kV, 30 mA) using CuK $\alpha$  radiation ( $\lambda$ = 0.154 nm) in the 2 $\theta$  range of 5–70°. The surface topography of the different solids was observed using SEM on a Hitachi S-4800 microscope. The energy dispersive spectrometer (EDS), SAMx Diode: SiLi, marque: NORAN was used for the determination of the catalyst chemical composition. FTIR spectra of the nanocomposite materials in the range 400–4000 cm<sup>-1</sup> were collected on a BRUKER ALPHA Platinum-ATR. Ultraviolet visible (UV–vis) absorbance spectrum was recorded at room temperature on a Specord 210 Analytik Jena spectrometer.

## 3. Results and discussion

### 3.1. Catalyst characterization

The diffraction patterns of the  $\text{CaCO}_3$  and  $\text{CuCO}_3\text{-CuO}$  obtained at different concentration of  $\text{Cu}(\text{NO}_3)_2$  are given in Fig.2. The XRD pattern of  $\text{CaCO}_3$  obtained from cuttlefish bone is assigned to the aragonite structure. In fact, the diffraction peaks appearing in the range of  $2\theta=26.8\text{--}27.6^\circ$ ,  $2\theta=33.3\text{--}38.7^\circ$ ,  $2\theta=43.5\text{--}46.4^\circ$ ,  $2\theta=49.1\text{--}51^\circ$  and  $2\theta=53.3$ , are well matched with the standard pattern of the aragonite structure according to the literature.<sup>45</sup> For the case of cuttlefish bone ( $\text{CaCO}_3$ ) modified with different concentrations of  $\text{Cu}(\text{NO}_3)_2$ , we note that there was appearance of two different phases, the first one diffraction peaks appear between  $2\theta=12.9^\circ$ ,  $2\theta=21.6\text{--}24.7^\circ$ ,  $2\theta=32.4\text{--}33.7^\circ$ ,  $2\theta=36.8^\circ$ ,  $2\theta=40.1^\circ$ ,  $2\theta=42.4^\circ$  and  $2\theta=44.1^\circ$  which correspond to a structure of copper carbonate  $\text{CuCO}_3$ , in agreement with the literature.<sup>46</sup> The second phase is related to the  $\text{CuO}$  structure and its diffraction peaks appear between  $2\theta=35.8$ ,  $2\theta=49.7^\circ$ ,  $2\theta=52.2$  and  $2\theta=53.9^\circ$  once again these results are consistent with the literature.<sup>46,47</sup> The figure also shows that the peaks intensity of  $\text{CuO}$  is much lower compared to peaks characteristic of  $\text{CuCO}_3$  phase.

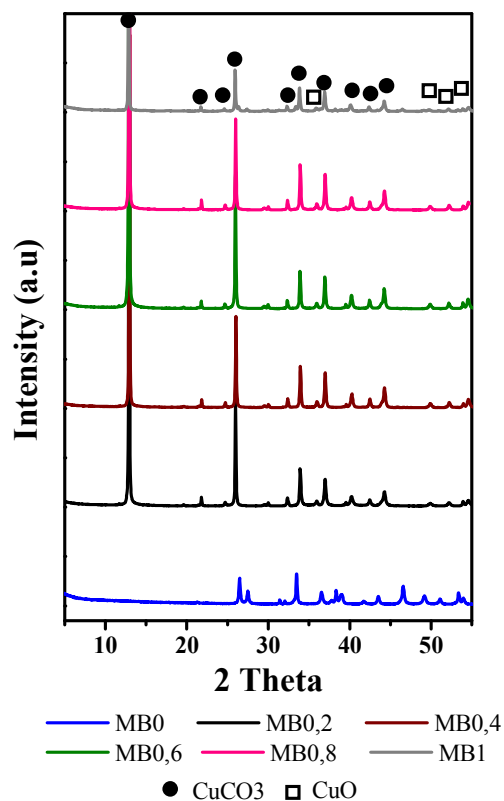


Fig.2. XRD patterns of CaCO<sub>3</sub> and CuCO<sub>3</sub>-CuO with different Cu concentration.

The appearance of CuO can be explained by the drying temperature (80°C) which as demonstrated by Teo et al, plays a very important role on the decomposition of CuCO<sub>3</sub> into CuO structure, and when increasing temperature CuO formation is expected to be enhanced.<sup>31</sup> We note also that the concentration of copper plays a very important role on the structure of the material CuCO<sub>3</sub>-CuO, the highest peaks intensity is obtained with average concentrations of Cu(NO<sub>3</sub>)<sub>2</sub> (the case of materials MB0.4 and MB0.6).

UV-vis reflectance diffuse spectra were recorded to investigate the coordination environment of Cu species. Fig.3 shows the UV-vis spectra of CaCO<sub>3</sub> and CuCO<sub>3</sub>-CuO with various Cu contents spanning from 200 nm to 1000 nm. All the materials exhibited intensive absorption centering around 282 nm for the case of CaCO<sub>3</sub> and



257-326 nm for  $\text{CuCO}_3$ , evidencing ligand-to-metal charge transfer between oxygen ligand and isolated  $\text{Cu}^{++}$ .<sup>48,49</sup>

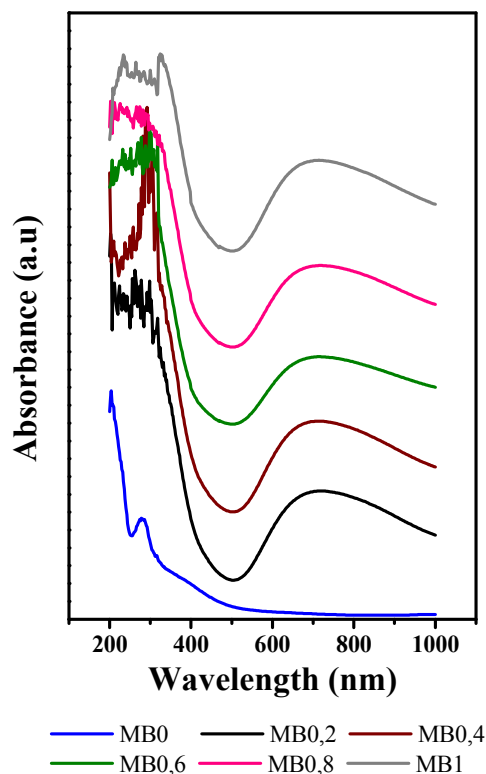
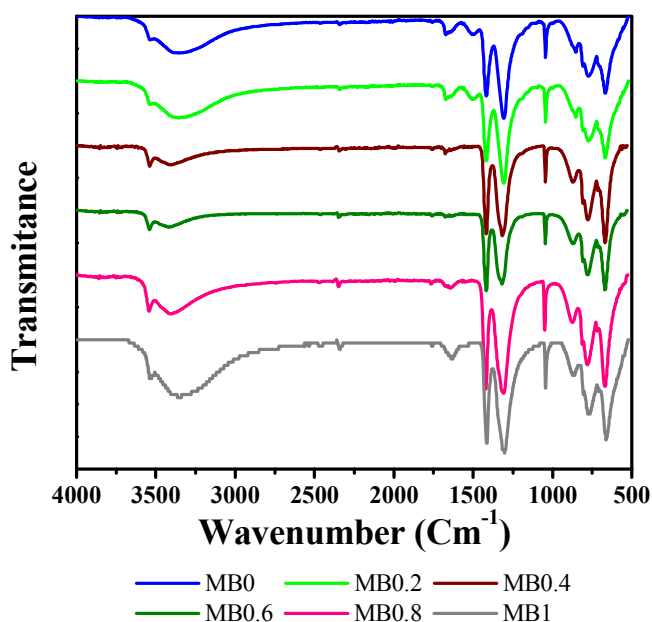


Fig.3. UV-vis spectra of  $\text{CaCO}_3$  and  $\text{CuCO}_3\text{-CuO}$  with different Cu concentration. The intensity of this last band increased proportionally with the Cu loading, suggesting more isolated  $\text{Cu}^{++}$  present in the composite  $\text{CuCO}_3\text{-CuO}$ . Furthermore a weak and broad absorption between 600 and 800 nm for all  $\text{CuCO}_3$  materials was generally assigned to the d-d transition of  $\text{Cu}^{++}$  in pseudo-octahedral coordination, indicating formation of segregated  $\text{CuO}$  particles.<sup>49,50</sup> The much higher intensity of the peak between 230–300 nm, compared to the peak across the range 600–800 nm, demonstrates that isolated  $\text{Cu}^{++}$  for  $\text{CuCO}_3$  phase are the predominant species in these materials. These results are consistent with XRD data.

The FTIR data of  $\text{CaCO}_3$  aragonite and  $\text{CuCO}_3\text{-CuO}$  composite obtained at different  $\text{Cu}(\text{NO}_3)_2$  concentration are given in Fig.4. For the case of  $\text{CaCO}_3$  aragonite we can

observe bands at  $1673\text{--}1504\text{ cm}^{-1}$  (overtones and combinations bands) attributed to the C=O groups of the carbonate ions.<sup>51</sup> The bands at  $1423\text{--}1310\text{ cm}^{-1}$  (antisymmetric stretching mode),  $1045\text{ cm}^{-1}$  (symmetric stretching mode),  $852\text{--}806\text{ cm}^{-1}$  (out of plane bending mode) and  $770\text{--}666\text{ cm}^{-1}$  (in plane bending mode) are attributed to the vibrations of carbonate internal group C–O corresponding to aragonite structure.<sup>52</sup> If the adsorption band of O–H stretching vibration around  $3542\text{ cm}^{-1}$  can be assigned to the presence of occluded water in  $\text{CaCO}_3$  aragonite, this adsorption peak with a shoulder at  $3335\text{ cm}^{-1}$  should be the O–H stretching vibration of crystal water and inter-particle hydrogen bonds.



**Fig.4.** FT-IR spectra of  $\text{CaCO}_3$  and  $\text{CuCO}_3\text{-CuO}$  with different Cu concentration.

The copper modified materials show some significant differences, indicating that physical and/or chemical changes occurred after copper adsorption. First, new peaks appear at  $1538$ ,  $2342$  and  $2464\text{ cm}^{-1}$ , whereas the one peak at  $1495\text{ cm}^{-1}$  disappears. Second, there is slight post-adsorption increase for peak strength at  $1538$ ,  $2342\text{ cm}^{-1}$  (Fig.4). These IR spectra changes are most likely due to the ion-exchange between

$\text{Cu}^{++}$  and  $\text{Ca}^{++}$ . We also note that there was an increase in the band intensity between 3360–3542 (the case of MB1 sample) due to the water absorbed in the surface of solids. On the other hand, there was a slight displacement a few bands between 661 and 1636  $\text{cm}^{-1}$ , suggesting that the conjugate action from the solids may be affected by the ion-exchange or electrostatic attraction on the surfaces during the adsorption process.

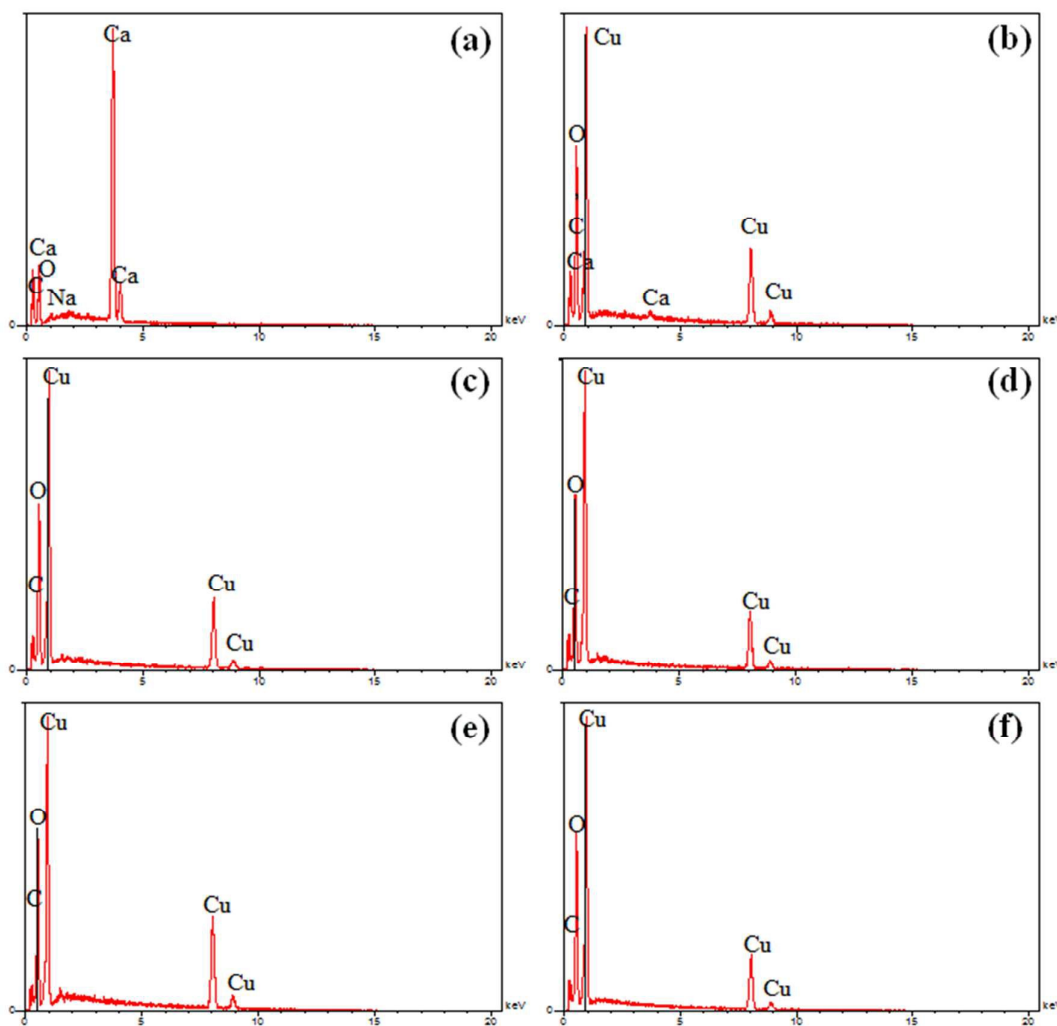


**Fig.5.** EDS of  $\text{CaCO}_3$  and composite  $\text{CuCO}_3\text{-CuO}$  with different Copper concentration ; (a) MB0, (b) MB0.2, (c) MB0.4, (d) MB0.6, (e) MB0.8, (f) MB1.

The chemical composition of the solids was characterized by EDS measurements to confirm the presence of  $\text{CaCO}_3$  and  $\text{CuCO}_3\text{-CuO}$ . The corresponding EDS spectrum of the different samples are shown on figure 5. Fig.5a presents the EDS spectra of MB0 sample which confirms the presence of  $\text{CaCO}_3$  with no other impurities. Concerning the  $\text{CaCO}_3$  modified by different concentrations of copper (MB0.4-MB1) Fig. 5c-f, we note that the increase in the copper concentration causes increased copper content in the solid structure (Fig. 5c-f). The tested concentrations generate the formation of a solid without any impurity, the resulting solids consisting essentially of C, Cu and O, except in the case of the solid MB0.2 which is formed by Ca, Cu, C and O, an obvious explanation of this is that the formation of a solid which contains both  $\text{CaCO}_3$  and  $\text{CuCO}_3\text{-CuO}$  with the  $\text{CuCO}_3\text{-CuO}$  being the predominant species (Fig. 5c).

Scanning electronic microscopy was used for the study of the morphology of the prepared materials. Fig.6 shows SEM images of MB0 (pure  $\text{CaCO}_3$ ) and modified with different concentrations of copper, which was obtained following precipitation method (see experimental part). There is a major difference in the morphology of the MB0 (pure  $\text{CaCO}_3$ ) and the MB0.2-MB1 ( $\text{CuCO}_3\text{-CuO}$ ) materials as obtained by the precipitation method. Fig.6a shows the image of cuttlefish bone (aragonite  $\text{CaCO}_3$ ), we can see that the nanostructure looks as noodle-like morphology, (Fig.6c-f) shows the SEM images of  $\text{CuCO}_3\text{-CuO}$  nanoplates with the thickness of platelets below 200 nm for MB0.6 (Fig.6d) and lateral dimensions much bigger in comparison with the thickness (Fig.6c-f), these results are significantly similar to the literature, we also note that the changes in the morphologies depends on the increasing of copper concentration. As it can be seen from (Fig.6d-f) higher concentrations of copper generates a spectacular morphologies in the case of MB1 (shape salad) and MB0.8

(shape desert rose). For the case of MB0.2 we observe that there is a mixture of aggregates that is due to the presence of several structures such as  $\text{CaCO}_3$  and the composite  $\text{CuCO}_3\text{-CuO}$  (Fig.6b), these results were already confirmed by EDS analysis. The obtained information indicates that the copper concentration has a significant influence on the morphology, and the connectivity of different nanoplates.

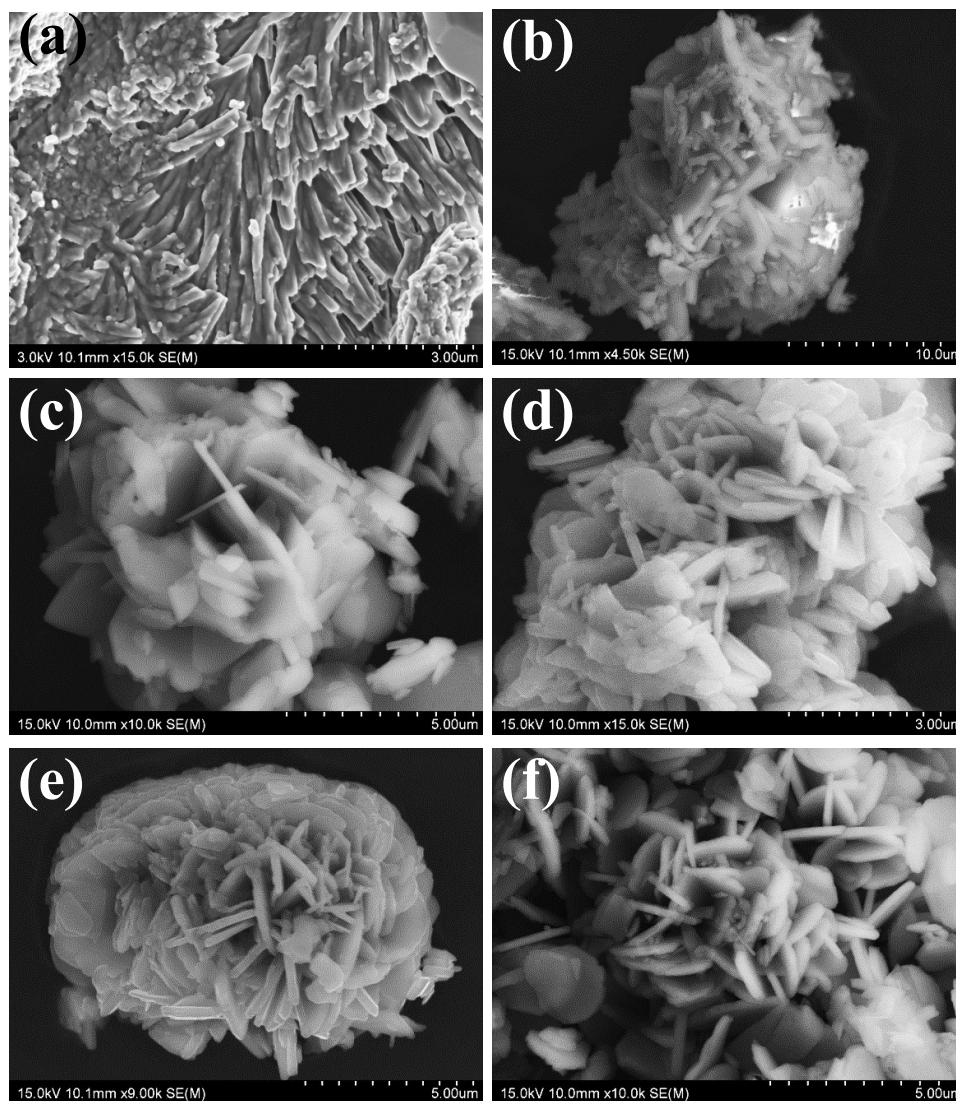


**Fig.6.** SEM image of  $\text{CaCO}_3$  and  $\text{CuCO}_3\text{-CuO}$  for different Copper concentration: (a) MB 0, (b) MB 0.2, (c) MB 0.4, (d) MB 0.6, (e) MB 0.8, (f) MB 1.

### 3.2. Catalytic experiments

Based on the results obtained in Fig.7.a and b we note that all the catalysts have a significant catalytic activity for the cycloaddition reaction except for the material  $\text{CaCO}_3$ .

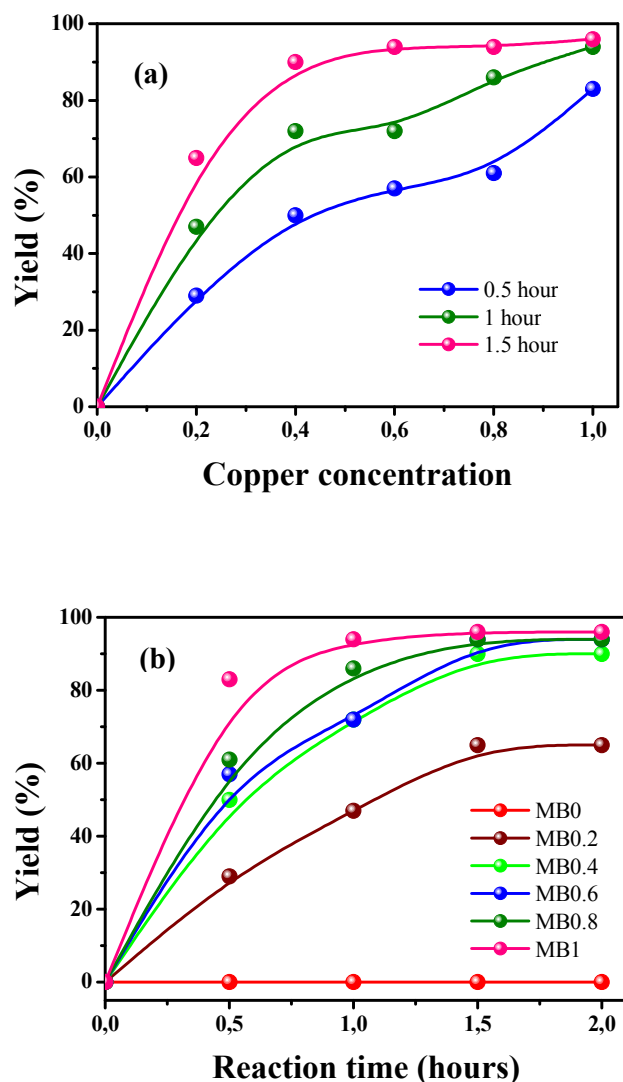


**Fig.7.** Optimization of parameters for cycloaddition reaction: (a) effect of copper concentration – 20mol% of catalyst; (b) effect of reaction time.

The catalyst prepared at high concentrations of copper possesses the best catalytic reactivity for cycloaddition reaction (case of MB1 and MB0,8), whereas when using  $\text{CuCO}_3\text{-CuO}$  solids interesting yields of about 96% are obtained for a reaction time

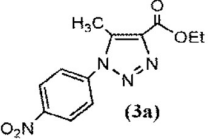
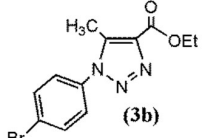
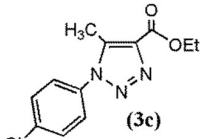
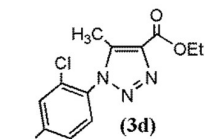
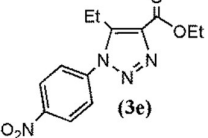
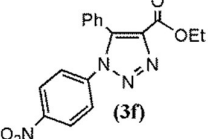
between 0.5-1.5 hours. Whereas, when using  $\text{CaCO}_3$  no product has been obtained, this difference in activity is thus probably due to the presence of  $\text{Cu}^{++}$  in composite materials which has been obtained by cation exchange with  $\text{Ca}^{++}$ . We note that not only we reduce the reaction time, but also we have developed a simple process for the separation of final product by filtration.

We also studied the effect of solvent on the cycloaddition reaction, hence without the addition of morpholine, no product was obtained with the composite materials (see table S1 additional file) as catalysts which indicates that the presence of morpholine plays a very important role for activated alkenes. It is well known that the nitrogen bases are used to accelerate triazole formation, in particular by coordinating to the catalytically active copper species, and promoting their liberation from the catalyst matrix, thus as improving their thermodynamic stability.<sup>53,54</sup> Moreover, the basic character of the amines can contribute to the deprotonation of the alkynes and alkenes component.<sup>55,56</sup>

If we compare our results with or without  $\text{CuCO}_3\text{-CuO}$  catalysts, the composite materials  $\text{CuCO}_3\text{-CuO}$  gives the best catalytic performance for this reaction (see Table.1). The addition of active methylene, arylazides and DMF in the presence of morpholine without  $\text{CuCO}_3\text{-CuO}$  materials leads to the formation of triazoles with interesting yields after 24 hours of reaction time. The different obtained structures of heterocycles were characterized by NMR spectroscopic analysis (NMR- $\text{H}^+$  and NMR- $\text{C}^{13}$ ) and the fourier transform infrared spectroscopy (FTIR) (see additional file). In all cases with or without catalysts composite we note that the halogen-substituted azides (Cl or Br) give moderate yields for the products (3b and 3c), because of the lower electroattractor nature of Cl and Br as compared to the nitro group.



**Table.1.** Cycloaddition reaction of arylazide 1(a-c) with the activated alkenes 2(a-d) performed at room temperature

Entry	R(1)	R'(2)	Product (3)	Without CuCO <sub>3</sub> -CuO <sup>a</sup>		With CuCO <sub>3</sub> -CuO <sup>b</sup>	
				Yield(%) <sup>c</sup>	t(h)	Yield(%) <sup>c</sup>	t(h)
1	Me (1a)	4-NO <sub>2</sub> (2a)	 (3a)	90	24	96	1.5
2	Me (1a)	4-Br (2b)	 (3b)	64	24	40	2
3	Me (1a)	4-Cl (2c)	 (3c)	61	24	60	4
4	Me (1a)	2-Cl,4-NO <sub>2</sub> (2d)	 (3d)	90	24	90	1.5
5	Et (1b)	4-NO <sub>2</sub> (2a)	 (3e)	80	24	79	1.5
6	Ph (1c)	4-NO <sub>2</sub> (2a)	 (3f)	89	24	93	1.5

<sup>a</sup>Reaction conditions: arylazide 1(a-c) (1 mmol), activated alkene 2(a-d) (1 mmol), Morpholine (1 mmol), DMF (1 mL), room temperature, 24 h (see procedure 1-S3).

<sup>b</sup>Reaction conditions: arylazide 1(a-c) (1 mmol), activated alkene 2(a-d) (1 mmol), Morpholine (1 mmol), CuCO<sub>3</sub>-CuO (20 mol%), DMF (1 mL), room temperature, (1,5-4) h (see procedure 2-S3).

<sup>c</sup>Isolated yields.



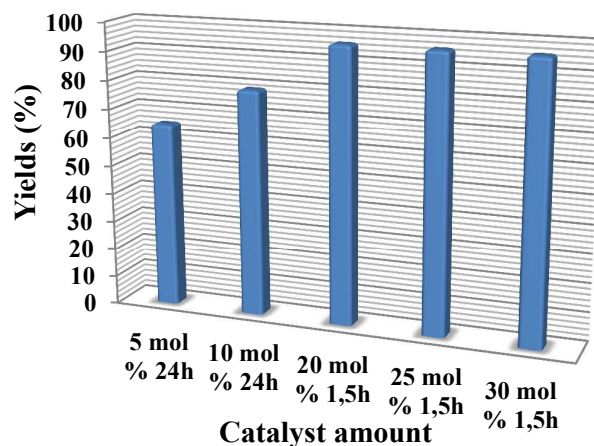


**Fig.8.** Effect of the catalysts amount in the catalytic reaction: nitrophenylazides (1mmol) in DMF (1mL), Ethyl aceto-acetate (1mmol),morpholine (1mmol) and  $\text{CuCO}_3\text{-CuO}$  (20mol%).

In order to understand the influence of the heterogeneous catalysts on the cycloaddition reaction, we have prepared a solution which contains nitrophenylazide (1mmol) in DMF (1mL), Ethyl aceto-acetate (1mmol) and morpholine (1mmol) using different amounts of composite catalysts  $\text{CuCO}_3\text{-CuO}$  (MB1) (Fig.8). Using 5 and 10 mol% of composite materials led to medium yields between 65-79% for 24 h reaction time. However we can notice in Fig. 8 that increasing the amount of catalyst has a positive impact on the reaction yield, with an optimal value (96%) obtained after 1.5 hour in the presence of 20-30% of catalyst.

In order to understand what is the catalytic active phase  $\text{CuCO}_3$  or  $\text{CuO}$ , we proposed to use the best catalyst MB1 at different temperature of calcination (200, 300, 400 and 500°C) to get different form of copper, the obtained solids were characterized by XRD and FTIR as shown in Fig.9. and Fig.10.

The results obtained by XRD for MB1 material treated at different temperatures of calcination shows that at 200 °C there is always the existence of two phases  $\text{CuCO}_3$  and  $\text{CuO}$ , with the appearance of all characteristic peaks of the  $\text{CuCO}_3$  phase (Fig.9),

but beyond of this value, we see the apparition of a single phase corresponding to CuO, these results are consistent with the literature.<sup>31</sup> When can also deduce that a temperature of 300°C is sufficient to transform all the copper carbonates to CuO.

Fig.10 represents the FTIR spectrum of CuCO<sub>3</sub>-CuO treated at different temperatures. The FTIR analysis are in agreement with the XRD results, the material MB1 before and after calcination at 200 °C presents the same vibration (existence of CuCO<sub>3</sub> and CuO), whereas for calcined materials between 300-500 °C, there has been a change in the vibration bands, we note the appearance of bands at 521 and 603 cm<sup>-1</sup> which correspond to the stretching vibration of Cu–O bond in monoclinic CuO.<sup>57</sup> The vibration in the range of 600–1166 cm<sup>-1</sup> (at 800 and 875 cm<sup>-1</sup>) is attributed to M–O stretching of CuO (M = Cu).<sup>58</sup> Further, a small and wide band at 1418 and 3271 cm<sup>-1</sup> is ascribed to the vibrational modes of O–H bond of the H<sub>2</sub>O molecules physisorbed on the surface of the CuO.<sup>59</sup>

The obtained material MB1 at different temperatures of calcination was used as catalyst for the reaction of arylazide 1(a) with activated alkene 2(a), the main results are listed in the table.2. From these results, we can conclude that the increase in the calcination temperature causes the formation of CuO particles, which their presence in the reaction medium has no effect on the reaction, thus the active phase in the reaction is copper carbonate CuCO<sub>3</sub>.

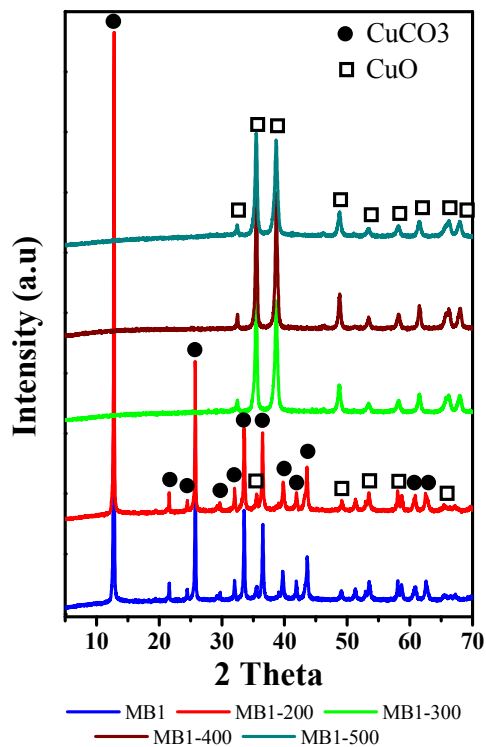


Fig.9. The XRD patterns of CuCO<sub>3</sub>-CuO calcined at different temperatures.

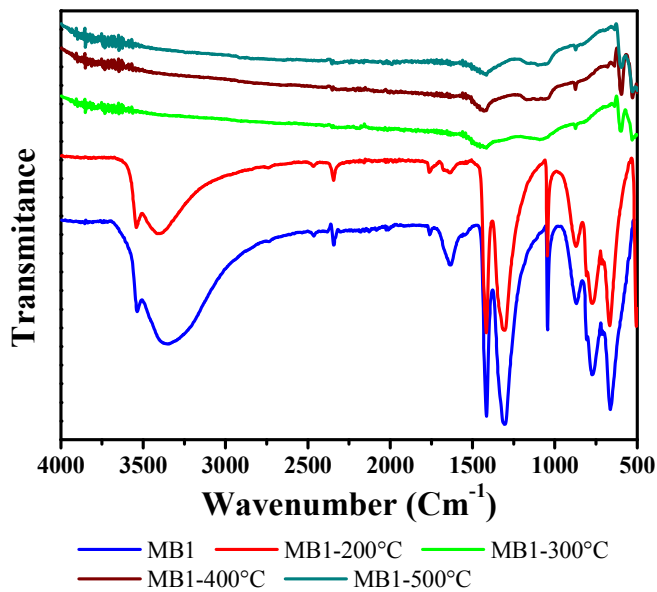


Fig.10. FT-IR spectra of CuCO<sub>3</sub>-CuO calcined at different temperatures.

**Table.2.** Effect of calcination temperature on the catalytic activity of the MB1 catalyst:

Catalysts	Temperature of calcination <sup>a</sup>	Phase	Yields
<b>MB1</b>	//	CuCO <sub>3</sub> -CuO	96
<b>MB1-200</b>	200 °C	CuCO <sub>3</sub> -CuO	54
<b>MB1-300</b>	300 °C	CuO	no product
<b>MB1-400</b>	400 °C	CuO	no product
<b>MB1-500</b>	500 °C	CuO	no product
<b>CuO</b> <sup>b</sup>	//	CuO	no product

<sup>a</sup> The catalysts were calcined for 2 hours.

<sup>b</sup> CuO commercial SIGMA-ALDRICH.

Reaction conditions: arylazide **1(a)** (1mmol), activated alkene **2(a)** (1mmol), Morpholine catalyst (20mol%), DMF (1mL), room temperature, 1,5 h.

Reusability of the catalysts has been studied in the cycloaddition of 4-nitrophenyl azide (**1**) under the following conditions: 4-nitrophenyl azide (2 mmol), Ethyl acetate (2 mmol), CuCO<sub>3</sub>-CuO (MB1, 20 mol%), DMF (2 ml), room temperature, 1.5 h reaction time. The catalysts were filtered, washed with DMF and dried before use in the following cycles, the results are represented in Fig.11 and as it can be seen the catalyst could be reused up to three times with little loss of activity, the slight decrease in yields may be due to the surface deactivation of nanocomposite CuCO<sub>3</sub>-CuO. We also note that the blue coloration of the catalyst before reaction, changed to a green color after 3 cycles of re-use due to the complexation of the catalysts with organic ligands in the reaction medium, these results were confirmed by XRD and FTIR analysis (see additional file Fig S1 and Fig S2). From the fourth cycle there was a progressive decrease in yields, in this stage we noticed that there was leaching of copper and the recovered catalyst lost its color due to the participation of copper in the reaction medium (see additional file Fig S3).

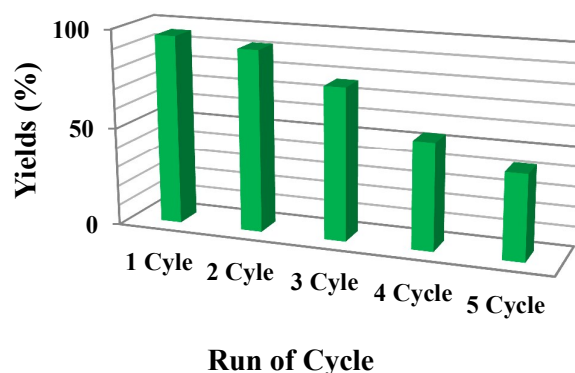


**Fig.11.** Catalyst reusability. Reaction conditions 4-nitrophenyl azide (2mmol), Ethyl aceto-acetate (2mmol), catalyst (20mol %), DMF (2 mL), room temperature, reaction time: 1.5 h (15 min) (at the end of the reaction, the catalyst is dried and reused).

### Conclusion:

The composite materials  $\text{CuCO}_3\text{-CuO}$  have been successfully prepared by direct synthesis method using  $\text{Cu}(\text{NO}_3)_2$  and bone of cuttlefish. The method involves the use of natural source for the preparation of efficient and low cost catalysts. The characterization methods show that the products formed by the precipitation have nanocomposite structure consisting of copper carbonate and copper oxide. The composites prepared at different copper concentrations show interesting results as catalysts for cycloaddition reaction and the increase of the copper content in the material leads to better results in the cycloaddition reaction, hence the MB1 nanocomposite material gives the best yield achieved in a short reaction time (1 hour). We have confirmed that the increase of the calcination temperature causes the formation of  $\text{CuO}$ , and a calcination about  $300\text{ }^\circ\text{C}$  is sufficient for the transformation of all  $\text{CuCO}_3$  to  $\text{CuO}$  phase. The use of MB1 at different temperatures of calcination allowed us to determine the active phase which is  $\text{CuCO}_3$ .

We showed that the reaction time, nature of used azide, and the catalyst mass play an important role on the yields of the product, and these catalyst may be used for three

cycles beyond of this value a decrease in yield has been obtained due to leaching of copper in the reaction medium.

## References

1. M. Olivares-Marín, E.M. Cuerda-Correa, A. Nieto-Sánchez, S. García, C. Pevida, S. Román, *Chemical Engineering Journal*, 2013, **217**, 71–81.
2. G. Wang, W. Xu. *Polymer Degradation and Stability*, 2013,**98**, 2323–2330.
3. K. De Witte, V. Meynen, M. Mertens, O.I. Lebedev, G. Van Tendeloo, A. Sepúlveda-Escribano, F. Rodríguez-Reinoso, E.F. Vansant, P. Cool, *Applied Catalysis B: Environmental*, 2008, **84**, 125–132.
4. Y-X. Zhou, Q. Zhang, J-Y. Gong, S-H. Yu, *J Phys Chem C*, 2008, **112**, 13383.
5. X. Ma, Q. Sun, X. Feng, X. He, J. Guo, H. Sun, H. Cao, *Applied Catalysis A: General*, 2013, **450**, 143–151.
6. M. Wang, HK. Zou, L. Shao, JF. Chen, *Powder Technol*, 2004, **142**, 166–74.
7. D. Liu, MZ. Yates, *Langmuir*, 2006, **22**, 5566.
8. N. Gehrke, H. Colfen, N. Pinna, M. Antonietti, N. Nassif, *Cryst Growth Des*, 2005, **5**, 1317.
9. W. Zhang, X. Li, Z. Qu, Q. Zhao, G. Chen, *Materials Letters*, 2010, **64**, 71–73.
10. X. Chen, C. Li, J. Wang, J. Li, X. Luan, Y. Li, R. Xu, B. Wang. *Materials Letters*, 2010, **64**, 1437–1440.
11. J. Lu, J.J. Bravo-Suárez, M. Haruta, S.T. Oyama. *Applied Catalysis A: General*, 2006, **302** 283–295.
12. G. Galán Muciño, R. Romero, A. Ramírez, S. Luz Martínez, R. Baeza-Jiménez, R. Natividad. *Fuel*, 2014, **138**143–148.

13. L-S. Hsieh, U. Kumar, J.C.S. Wu, *Chemical Engineering Journal*, 2010, **158**, 250–256.
14. W. Wei Sheng Ho, H. Kiat Ng, Suyin Gan, *Bioresource Technology*, 2012, **125**, 158–164.
15. Minfeng Zeng, Yijun Du, Chenze Qi, Shufeng Zuo, Xiudong Li, Linjun Shao and Xian-Man Zhang. *Green Chem*, 2011, **13**, 350.
16. C-T. Hsieh, Y-T. Lin, J-Y. Lin, J-L. Wei, *Materials Chemistry and Physics*, 2009, **114**, 702–708.
17. B. Gao, L. Liu, J. Liu, F. Yang, *Applied Catalysis B: Environmental*, 2013, **138–139**, 62–69.
18. Myriam A.M. Motchelaho, Haifeng Xiong, Mahluli Moyo, Linda L. Jewell, Neil J. Coville. *Journal of Molecular Catalysis A: Chemical*, 2011, **335**, 189–198.
19. S-l. Fu, Q. Song, Q. Yao, *Chemical Engineering Journal*, 2015, **262**, 9–17.
20. C. Wang, C. He, Z. Tong, X. Liu, B. Ren, F. Zeng, *International Journal of Pharmaceutics*, 2006, **308**, 160–167.
21. C. Qin, B. Feng, J. Yin, J. Ran, L. Zhang, V. Manovic, *Chemical Engineering Journal*, 2015, **262**, 665–675.
22. I. Takahara, K. Murata, K. Sato, Y. Miura, M. Inaba, Y. Liu, *Applied Catalysis A: General*, 2013, **450**, 80–87.
23. B. Yao, Z. Ding, X. Feng, L. Yin, Q. Shen, Y. Shi, J. Zhang, *Electrochimica Acta*, **2014**, **148**, 283–290.
24. K. Zhang, S. Wu, X. Wang, J. He, B. Sun, Y. Jia, T. Luo, F. Meng, Z. Jin, D. Lin, W. Shen, L. Kong, J. Liu, *Journal of Colloid and Interface Science*, 2015, **446**, 194–202.

25. F. M. Hossain, B.Z. Dlugogorski, E.M. Kennedy, I.V. Belova, Graeme E. Murch, *Solid State Communications*, 2010, **150**, 848–851.
26. G. Stavbera, Z. Časar, *Appl. Organometal. Chem*, 2013, **27**, 159–165.
27. M. Casielloa, A. Monopoli, P. Cotugno, A. Milella, M. Michela Dell’Anna, F. Ciminale, A. Nacci, *Journal of Molecular Catalysis A: Chemical*, 2014, **381**, 99–106.
28. F. Yu, F. Li, B. Zhang, H. Li, L. Sun, *ACS Catal*, 2015, **5**, 627–630.
29. M.H. Habibi, B. Karimi, *Journal of Industrial and Engineering Chemistry*, 2014, **20**, 925–929.
30. J-M. Sun, X-H. Zhao, J-C. Huang, *Chemosphere*, 2005, **58**, 1003–1010.
31. C-H. Teo, Y. Zhu, X. Gao, A.T-S. Wee, C-H. Sow, *Solid State Communications*, 2008, **145**, 241–245.
32. S. Güniz Küçükgülzel, Pelin Çıkla-Süzgün, *European Journal of Medicinal Chemistry*, 2015, **97**, 830–870.
33. K. Tamura, K. Inoue, M. Takahashi, S. Matsuo, K. Irie, Y. Kodama, T. Gamo, S. Ozawa, M. Yoshida, *Food and Chemical Toxicology*, 2015, **78**, 86–95.
34. J. Flieger, M. Tatarczak-Michalewska, M. Wujec, M. Pitucha, R. Świeboda, *Journal of Pharmaceutical and Biomedical Analysis*, 2015, **107**, 501–511.
35. S. Mahdieh Hashemi, H. Badali, H. Irannejad, M. Shokrzadeh, S. Emami, *Bioorganic & Medicinal Chemistry*, 2015, **23**, 1481–1491.
36. R. Huisgen, *Angew. Chem*, 1963, **75**, 604–637.
37. V.V. Rostovtsev, L.G. Green, V.V. Fokin, K.B. Sharpless, *Angew. Chem. Int. Ed*, 2002, **41**, 2596–2599.
38. B. Boukoussa, S. Zeghada, G. Bentabed Ababsa, R. Hamacha, A. Derdour, A. Bengueddach, F. Mongin, *Applied Catalysis A General*, 2015, **489**, 131–139.



39. S. Roy, T. Chatterjee, M. Pramanik, A.S. Ro, A. Bhaumik, Sk. Manirul Islam, J. Mol.Catal. A: Chem, 2014, **386**, 78–85.
40. I. Jllia, F. Gallier, N. Brodie-Linder, J. Uziel, J. Augé, N. Lubin-Germain, J. Mol.Catal. A: Chem, 2014, **393**, 56–61.
41. M. Nasrollahzadeh, S. Mohammad Sajadi, Journal of Colloid and Interface Science. 457 (2015) 141–147.
42. M. Nasrollahzadeh, S. Mohammad Sajadi, A. Rostami-Vartooni, M. Khalaj, Journal of Colloid and Interface Science, 2015, **453**, 237–243.
43. K. Martina, S.E.S. Leonhardt, B. Ondruschka, M. Carini, A. Binello, G. Cravotto, J.Mol. Catal. A: Chem, 2011, **334**,60–64.
44. T.R. Chan, V.V. Fokin, QSAR Comb. Sci, 2007 , **26**, 1274–1279.
45. A. Ben Nasr, K. Walha, C. Charcosset, R. Ben Amar. Journal of Fluorine Chemistry, 2011,**132**, 57–62.
46. W.N.R. Wan Isahak, Z.A. Che Ramli, M. Wafiuddin Ismail, K. Ismail, R.M. Yusop, M.W. Mohamed Hisham, M. Ambar Yarmo, Journal of CO<sub>2</sub> Utilization, 2013, **2**, 8–15.
47. J-H. Kim, A. Katoch, S-W. Choi, S. Sub Kim, Sensors and Actuators B, 2015, **212**, 190–195.
48. H.T. Gomes, P. Selvam, S.E. Dapurkar, J.L. Figueiredo, J.L. Faria, Microporous Mesoporous Mater, 2005, **86**, 287–294.
49. S. Velu, L.Wang, M. Okazaki, K. Suzuki, S. Tomura, Microporous Mesoporous Mater, 2002, **54**, 113–126.
50. S. Sonia, I. Jose Annsi, P. Suresh Kumar, D. Mangalaraj, C. Viswanathan, N. Ponpandian, Materials Letters, 2015, **144**, 127–130.

51. S.-W. Lee, Y.-N. Jang, K.-W. Ryu, S.-C. Chae, Y.-H. Lee, C.-W. Jeon. *Micron*, 2011, **42**, 60–70.
52. F.Z. Zakaria, J. Mihaly, I. Sajo, R. Katona, L. Hajba, F.A. Aziz, J. Mink. *J. Raman Spectrosc*, 2008, **39**, 1204–1209.
53. M. Meldal, C.W. Tornøe, *Chem. Rev*, 2008, **108**, 2952–3015.
54. R. Berg, B.F. Straub, *Beilstein J. Org. Chem*, 2013, **9**, 2715–2750.
55. G.-C.Kuang, P.M. Guha, W.S. Brotherton, J.T. Simmons, L.A. Stankee, B.T. Nguyen, R.J. Clark, L. Zhu, *J. Am. Chem. Soc*, 2011, **133**, 13984–14001.
56. S. Zeghada, G. Bentabed-Ababsa, A. Derdour, S. Abdelmounim, L.R. Domingo, J.A. Saez, T. Roisnel, E. Nassar, F. Mongin, *Org. Biomol. Chem*, 2011, **9**, 4295–4305.
57. V.V.T. Padil, M. Cernik, *Int. J. Nanomed*, 2013, **8**, 889–898.
58. Y. Xu, D. Chen, X. Jiao, K. Xue, *Mater. Res. Bull*, 2007, **42**, 1723–1731.
59. A.N. Ejhieh, H.Z. Mobarakeh, *J Ind Eng Chem*, 2014, **20**, 1421–31.

